Inorganic Chemistry
Article

Inorg. Chem. **2010**, *49*, 8953–8961 **8953**
DOI: 10.1021/ic1013472

cis-2,2′-Bipyrimidine-Bridged Polynuclear Complex: A Stairway-like Mixed-Valent $\{Fe_4\}$ Cluster

Pablo Alborés* and Eva Rentschler*,†

Institut für Anorganische Chemie und Analytische Chemie, Johannes Gutenberg-Mainz Universität, Duesbergweg 10−14, D-55099 Mainz, Germany. † *E-mail: rentschl@uni-mainz.de. Tel: +54 (011) 4576-3380. Fax: +54 (011) 4576-3343.*

Received July 6, 2010

We report the first example of a polynuclear discrete coordination compound exhibiting only bpym bridges and containing a first-row d transition metal. A smooth self-assembly one-pot synthetic route, starting from simply $FeCl_2$ and $FeCl_3$ hydrates, allowed us to prepare a tetranuclear Fe_4 cluster with a stairway-like structure and the formula *cis*-$\{[(H_2O)Cl_3Fe^{III}$-μ(bpym)$Fe^{II}Cl_2]\}_2$-μ(bpym) (**1**) . All spectroscopic data suggest that complex **1** is a valence-localized mixed-valent $Fe^{II}-Fe^{III}$ cluster with typical Mössbauer lines for both sites, which do not change with temperature. Reflectance spectroscopy did not allow one to distinguish an intervalence charge-transfer band. However, time-dependent density functional theory (DFT) calculations predict a weak high-energy $Fe^{II} \rightarrow Fe^{III}$ transition. Regarding the magnetic properties, the high-spin Fe^{II} and Fe^{III} ions interact in a weakly antiferromagnetic way with isotropic *J* constants of only a few wavenumbers as derived from direct-current susceptibility and magnetization data. Broken-symmetry DFT calculations support these observations.

Introduction

2,2′-Bipyrimidine (bpym) is the key member of the pyridine-type bis-bidentate ligands capable of bridging two different metal ions. In spite of its versatility to link a great variety of transition metals, there are to date only reports either of just dinuclear complexes[1−4] or, on the contrary, of one-dimensional (1D) infinite chains, with bpym being the unique bridging moiety.[4−6] bpym has proven to mediate a moderate interaction between metal ions as evidenced from the electronic and magnetic properties of the dinuclear complexes. It also has been extensively used in combination with other bridging ligands in the design of two-dimensional (2D) and three-dimensional (3D) networks, mainly within the field of molecular-based magnets.[4,7,8] The preparation of homodinuclear bpym-bridged compounds and the design of 1D coordination polymers appear to be quite reasonable tasks. Changing the stoichiometry of the metal fragments and bpym leads to the dinuclear species when the metal ions are used in excess, whereas just mixing one to one amounts of the metal source and bridging ligand leads to the polymeric form. However, the preparation of discrete clusters with intermediate nuclearity size bridged by bpym seems to be a real synthetic challenge for chemists. In fact, to the best of our

*To whom correspondence should be addressed. Current address: INQUIMAE-DQIAyQF, Universidad de Buenos Aires, Ciudad Universitaria, Pabellón 2, 3 piso, Buenos Aires C1428EHA, Argentina. E-mail: albores@qi.fcen.uba.ar. Tel: +49 (0)6131 39 25491. Fax: +49 (0)6131 39 23922.

(1) (a) Brewer, G.; Sinn, E. *Inorg. Chem.* **1985**, *24*, 4580. (b) Real, A.; Zarembowitch, J.; Kahn, O.; Solans, X. *Inorg. Chem.* **1987**, *26*, 2939. (c) Demunno, G.; Julve, M.; Lloret, F.; Derory, A. *J. Chem. Soc., Dalton Trans.* **1993**, 1179. (d) Demunno, G.; Julve, M.; Verdaguer, M.; Bruno, G. *Inorg. Chem.* **1993**, *32*, 2215. (e) Demunno, G.; Julve, M.; Lloret, F.; Faus, J.; Caneschi, A. *J. Chem. Soc., Dalton Trans.* **1994**, 1175. (f) Schoberl, U.; Magnera, T. F.; Harrison, R. M.; Fleischer, F.; Pflug, J. L.; Schwab, P. F. H.; Meng, X. S.; Lipiak, D.; Noll, B. C.; Allured, V. S.; Rudalevige, T.; Lee, S.; Michl, J. *J. Am. Chem. Soc.* **1997**, *119*, 3907. (g) Baumann, F.; Stange, A.; Kaim, W. *Inorg. Chem. Commun.* **1998**, *1*, 305. (h) Sieger, M.; Vogler, C.; Klein, A.; Knodler, A.; Wanner, M.; Fiedler, J.; Zalis, S.; Snoeck, T. L.; Kaim, W. *Inorg. Chem.* **2005**, *44*, 4637. (i) Gaspar, A. B.; Ksenofontov, V.; Reiman, S.; Gutlich, P.; Thompson, A. L.; Goeta, A. E.; Munoz, M. C.; Real, J. A. *Chem.—Eur. J* **2006**, *12*, 9289. (j) Govindaswamy, P.; Canivet, J.; Therrien, B.; Suss-Fink, G.; Stepnicka, P.; Ludvik, J. *J. Org. Chem.* **2007**, *692*, 3664. (k) Inagaki, A.; Yatsuda, S.; Edure, S.; Suzuki, A.; Takahashi, T.; Akita, M. *Inorg. Chem.* **2007**, *46*, 2432.

(2) Demunno, G.; Ventura, W.; Viau, G.; Lloret, F.; Faus, J.; Julve, M. *Inorg. Chem.* **1998**, *37*, 1458.

(3) Sun, J. S.; Zhao, H. H.; Xiang, O. Y.; Clerac, R.; Smith, J. A.; Clemente-Juan, J. M.; Gomez-Garcia, C.; Coronado, E.; Dunbar, K. R. *Inorg. Chem.* **1999**, *38*, 5841.

(4) Thetiot, F.; Triki, S.; Pala, J. S.; Galan-Mascaros, J. R.; Martinez-Agudo, J. M.; Dunbar, K. R. *Eur. J. Inorg. Chem.* **2004**, 3783.

(5) Pointillart, F.; Herson, P.; Boubekeur, K.; Train, C. *Inorg. Chim. Acta* **2008**, *361*, 373.

(6) (a) Morgan, L. W.; Goodwin, K. V.; Pennington, W. T.; Petersen, J. D. *Inorg. Chem.* **1992**, *31*, 1103. (b) Demunno, G.; Viterbo, D.; Caneschi, A.; Lloret, F.; Julve, M. *Inorg. Chem.* **1994**, *33*, 1585. (c) Demunno, G.; Julve, M.; Real, J. A.; Lloret, F.; Scopelliti, R. *Inorg. Chim. Acta* **1996**, *250*, 81. (d) Cortes, R.; Urtiaga, M. K.; Lezama, L.; Pizarro, J. L.; Arriortua, M. I.; Rojo, T. *Inorg. Chem.* **1997**, *36*, 5016. (e) Demunno, G.; Poerio, T.; Julve, M.; Lloret, F.; Viau, G.; Caneschi, A. *J. Chem. Soc., Dalton Trans.* **1997**, 601. (f) Demunno, G.; Poerio, T.; Julve, M.; Lloret, F.; Faus, J.; Caneschi, A. *J. Chem. Soc., Dalton Trans.* **1998**, 1679. (g) Demunno, G.; Poerio, T.; Julve, M.; Lloret, F.; Viau, G. *New J. Chem.* **1998**, *22*, 299. (h) Armentano, D.; Demunno, G.; Guerra, F.; Faus, J.; Lloret, F.; Julve, M. *Dalton Trans.* **2003**, 4626.

Published on Web 08/31/2010

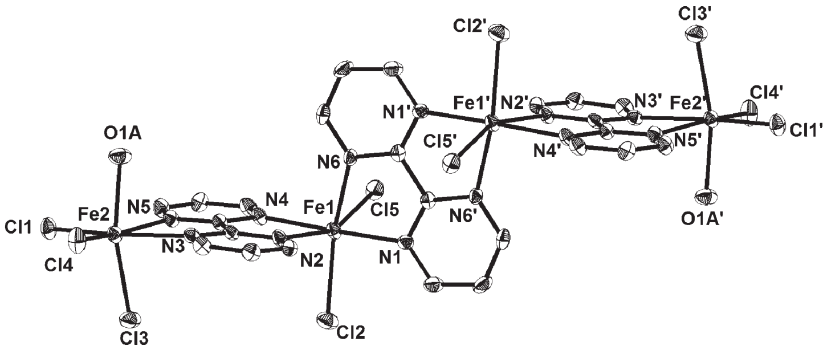

Figure 1. ORTEP representation (50% probability) of complex **1**. Hydrogen atoms were omitted for the sake of clarity. Symmetry-equivalent positions: $-x, -y, -z$.

knowledge, there is only one example reported to date of this type of molecule with full structural characterization, corresponding to a tetranuclear silver(I) compound of the formula $[Ag_4(hfac)_4(\mu_2\text{-bpym})_3]$.[5] No examples are available with first-row paramagnetic transition metals providing possibly interesting electronic and/or magnetic properties because of their variability of electronic and spin ground states.

In this work, we report the first example of a polynuclear discrete coordination compound exhibiting only bpym bridges and containing a first-row d transition metal. A smooth self-assembly one-pot synthetic route starting from $FeCl_2$ and $FeCl_3$ hydrates allows us to prepare a tetranuclear Fe_4 cluster, *cis*-$\{[(H_2O)Cl_3Fe^{III}\text{-}\mu(bpym)Fe^{II}Cl_2]\}_2\text{-}\mu(bpym)$ (**1**), with a stairway-like structure. The mixed-valent Fe^{II}/Fe^{III} character makes this novel compound even more interesting for chemists. We report herein its structural characterization and spectroscopic and magnetic properties, together with density functional theory (DFT) calculations, completing a deep study about this new bpym-bridged Fe_4 cluster.

Results and Discussion

Synthetic Procedure. The reaction of equimolar amounts of $FeCl_3$ and $FeCl_2$ hydrates with bpym in a methanol/acetonitrile mixture afforded single crystals of the mixed-valent cluster **1**, after a first removal of an insoluble polycrystalline solid, which as not further characterized. The high insolubility in acetonitrile of **1** drives the self-assembly process, which most probably involves the preformation of a previously characterized dinuclear compound *cis*-$(bpym)Cl_2Fe^{II}\text{-}\mu(bpym)Fe^{II}Cl_2(bpym)$.[3] Capping the latter with $Fe^{III}Cl_3$ units and an additional water solvent molecule, which completes the octahedral environment, ends in the cis tetranuclear Fe_4 species. This solid proves insoluble in all common solvents, with the exception of water, where it quickly decomposes.

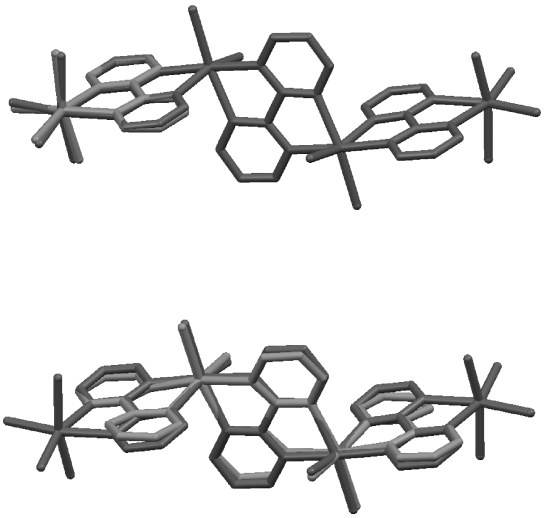

Figure 2. Atom-to-atom overlaying of crystal structure pairs: **1**/**2** (top) and **1**/**3** (bottom).

Structural Characterization. The X-ray structure of complex **1** reveals an all-cis configuration in an almost perfect stairway structure, with $\{Fe^{III}\text{-}\mu(bpym)\text{-}Fe^{II}\}$ motifs (related by a crystallographic inversion center) lying as each stair step (Figure 1). Alternatively, by a 90° rotation, it can be described as a longer staircase, with each Fe^{III} as the first and last stair steps and both Fe^{II} ions as the middle ones (see the Supporting Information, SI). Noticeably, as nice complements, structures are reported for the mononuclear complex $[Fe^{III}Cl_3H_2O(bpym)]$[2] (**2**) and the dinuclear complex *cis*-$[\{Fe^{II}(bpym)Cl_2\}_2\text{-}\mu(bpym)]$[3] (**3**). The Fe^{III} coordination sphere in **1** closely matches the observed one in complex **2**, while the Fe^{II} backbone resembles the full structure of complex **3**, as can be noticed from an atom-to-atom overlaying of both structures with root-mean-square (rms) values of 0.147 and 0.307 Å, respectively (Figure 2).

Overall, the whole structure of complex **1** can be viewed as a superposition of the crystal structures of complexes **2** and **3**. In terms of its architecture, complex **1** is built up

(7) (a) Demunno, G.; Julve, M.; Lloret, F.; Faus, J.; Verdaguer, M.; Caneschi, A. *Angew. Chem., Int. Ed. Engl.* **1993**, *32*, 1046. (b) Demunno, G.; Julve, M.; Nicolo, F.; Lloret, F.; Faus, J.; Ruiz, R.; Sinn, E. *Angew. Chem., Int. Ed. Engl.* **1993**, *32*, 613. (c) Decurtins, S.; Schmalle, H. W.; Schneuwly, P.; Zheng, L. M.; Ensling, J.; Hauser, A. *Inorg. Chem.* **1995**, *34*, 5501. (d) Demunno, G.; Julve, M.; Viau, G.; Lloret, F.; Faus, J.; Viterbo, D. *Angew. Chem., Int. Ed. Engl.* **1996**, *35*, 1807. (e) Demunno, G.; Poerio, T.; Viau, G.; Julve, M.; Lloret, F.; Journaux, Y.; Riviere, E. *Chem. Commun.* **1996**, 2587. (f) Armentano, D.; Demunno, G.; Lloret, F.; Julve, M. *Inorg. Chem.* **1999**, *38*, 3744. (g) Marshall, S. R.; Incarvito, C. D.; Manson, J. L.; Rheingold, A. L.; Miller, J. S. *Inorg. Chem.* **2000**, *39*, 1969. (h) Triki, S.; Thetiot, F.; Galan-Mascaros, J. R.; Pala, J. S. *New J. Chem.* **2001**, *25*, 954. (i) Armentano, D.; Demunno, G.; Lloret, F.; Julve, M.; Curely, J.; Babb, A. M.; Lu, J. Y. *New J. Chem.* **2003**, *27*, 161. (j) Colacio, E.; Debdoubi, A.; Kivekas, R.; Rodriguez, A. *Eur. J. Inorg. Chem.* **2005**, 2860. (k) Colacio, E.; Lloret, F.; Navarrete, M.; Romerosa, A.; Stoeckli-Evans, H.; Suarez-Varela, J. *New J. Chem.* **2005**, *29*, 1189. (l) Podgajny, R.; Pinkowicz, D.; Korzeniak, T.; Nitek, W.; Rams, M.; Sieklucka, B. *Inorg. Chem.* **2007**, *46*, 10416. (m) Baca, S. G.; Malaestean, I. L.; Keene, T. D.; Adams, H.; Ward, M. D.; Hauser, J.; Neels, A.; Decurtins, S. *Inorg. Chem.* **2008**, *47*, 11108. (n) Fabelo, O.; Pasan, J.; Lloret, F.; Julve, M.; Ruiz-Perez, C. *Inorg. Chem.* **2008**, *47*, 3568.
(8) Albores, P.; Rentschler, E. *Dalton Trans.* **2009**, 2609.
(9) Oshio, H.; Hoshino, N.; Ito, T.; Nakano, M. *J. Am. Chem. Soc.* **2004**, *126*, 8805.

Table 1. Crystal and Refinement Data

	1
empirical formula	$C_{24}H_{22}Cl_{10}Fe_4N_{12}O_2 \cdot 2H_2O$
fw	1124.47
temperature (K)	173
wavelength (Å)	0.710 69
cryst syst	monoclinic
space group	$P2_1/n$
unit cell dimensions	$a = 7.4691(3)$ Å
	$b = 11.7690(5)$ Å
	$c = 22.9889(10)$ Å
	$\beta = 96.8550(10)°$
volume (Å^3)	2006.4(2)
Z	2
density calcd (g cm^{-3})	1.861
abs coeff (mm^{-1})	2.133
$F(000)$	1120
cryst size (mm^3)	$0.12 \times 0.11 \times 0.05$
θ range (deg)	1.78−27.45
limiting indices	$-9 \le h \ge 9$
	$-15 \le k \ge 15$
	$-29 \le l \ge 29$
reflns collected	21 602
indep reflns	4563 [$R_{int} = 0.0389$]
completeness to θ (%)	99.5
refinement method	full-matrix least squares on F^2
data/restraints/params	4563/4/256
GOF on F^2	1.091
final R indices [$I > 2\theta(I)$]	R1 = 0.0345, wR2 = 0.0711
R indices (all data)	R1 = 0.0470, wR2 = 0.0781
largest diff peak and hole (e Å^{-3})	0.497 and −0.407

from the coordination of neutral $\{Fe^{III}Cl_3H_2O\}$ moieties to terminal bpym free sites of complex **2**.

As can be already realized from a comparison of the crystallographic data[2,3] of complexes **2** and **3**, in the case of complex **1**, a small but sizable difference can be found in the Fe−N bond distances for both metal oxidation states (average Fe^{III}−N distance, 2.241 Å; average Fe^{II}−N distance, 2.192 Å). The shorter Fe^{II}−N bond distance simply reflects the enhanced π-bonding ability of Fe^{II} versus Fe^{III} ions. On the other hand, the Fe−Cl bond distances are clearly shorter for Fe^{III} (average Fe^{III}−Cl distance, 2.281 Å; average Fe^{II}−Cl distance, 2.387 Å), as was expected from the combination of the chloride π-donor ligand with the better acceptor ion Fe^{III} in comparison with Fe^{II} (Table 2).

The coordinated aqua ligand exhibits a considerably shorter Fe^{III}−O bond distance than the one observed in complex **2**, 2.059(2) vs 2.130 Å, respectively. This is accompanied with a lengthening of the trans Fe−Cl distance [2.3230(8) vs 2.305 Å] compared to complex **2**.

Regarding the local symmetry of both Fe sites, they appear considerably distorted from an octahedron, with angles of 73.56(8)° (N3−Fe1−N5) and 106.99(3)° (Cl3−Fe2−Cl4). All of the metric data indicate localized Fe^{II} and Fe^{III} sites within this mixed-valent compound crystal structure, in agreement with the marked superposition of the solid-state structures of the Fe^{III}-only compound **2** and the Fe^{II}-only compound **3**.

In the crystal packing, the supramolecular organization of complex **1** is best described as adjacent tetranuclear clusters hold together by $\pi-\pi$ stacking between the outer bpym rings (mean ring−ring distance ca. 3.94 Å). Hydrogen bonding between coordinated water and the neighboring Fe^{II}−Cl4 (3.161 Å for O1···Cl4) completes the supramolecular arrangement (see the SI). Hence, with 6.708 Å, the shortest intercluster Fe···Fe distance ($Fe1_{neighbor1}$−$Fe2_{neighbor2}$) is considerably longer than the intracluster Fe−Fe distances (Fe1−Fe2 = 5.882 Å and Fe2−Fe2′ = 5.831 Å). These intermolecular interactions propagate along the structure, affording 2D sheets connected through a further hydrogen-bonding network involving the free water molecule, the coordinated aqua ligand, and coordinated Cl3 and Cl5 ligands (see the SI). An overall zigzag arrangement can be observed for the π-stacked sheets of Fe_4 complexes. A similar pattern has been observed in the crystal packing of the related dinuclear complex, $[\{FeCl_3(H_2O)\}_2\text{-}\mu(bpym)]^2$ (**4**). In this case, the intermolecular Fe···Fe distance is somewhat shorter, 6.422 Å.

Table 2. Selected Bond Lengths (Å) and Bond Angles (deg) for Complex **1**

Fe1−Cl1	2.2618(8)	N6−Fe2−Cl3	82.72(6)
Fe1−Cl2	2.2588(8)	N1−Fe2−Cl4	90.17(7)
Fe1−Cl5	2.3230(8)	N4−Fe2−Cl4	91.50(6)
Fe1−O1	2.059(2)	O1−Fe1−N3	82.01(9)
Fe1−N3	2.220(2)	N3−Fe1−Cl2	93.41(6)
Fe1−N5	2.263(2)	O1−Fe1−Cl2	92.32(7)
Fe2−Cl3	2.3668(8)	O1−Fe1−Cl1	90.96(7)
Fe2−Cl4	2.4081(8)	Cl2−Fe1−Cl1	102.98(3)
Fe2−N1	2.166(2)	O1−Fe1−N5	86.88(8)
Fe2−N2	2.201(2)	N3−Fe1− N5	73.56(8)
Fe2−N4	2.175(2)	Cl1−Fe1−N5	90.08(6)
Fe2−N6	2.225(2)	N3− Fe1−Cl5	86.53(6)
Fe1···Fe2	5.882	Cl2−Fe1−Cl5	94.95(3)
Fe2···Fe2′	5.831	Cl1−Fe1−Cl5	98.14(3)
		N5−Fe1−Cl5	83.54(6)
N1−Fe2−N2	75.67(8)	N2−Fe2−Cl4	92.18(7)
N4−Fe2−N2	101.04(8)	Cl3−Fe2−Cl4	106.99(3)
N1−Fe2−N6	102.83(9)	N2−Fe2−N6	81.80(8)
N4−Fe2−N6	74.99(8)		
N2−Fe2−N6	81.80(8)		
N1−Fe2−Cl3	91.50(6)		
N4−Fe2−Cl3	91.11(6)		

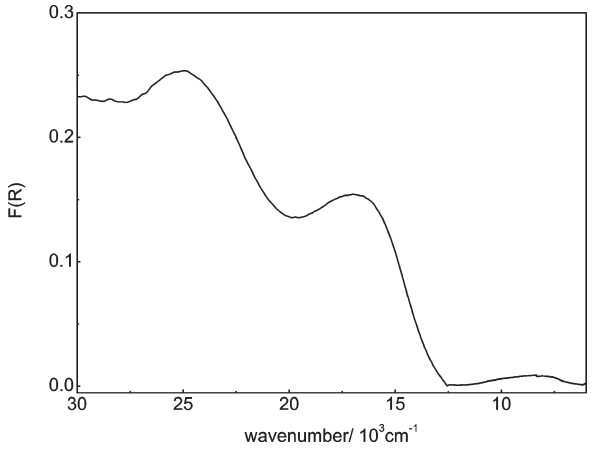

Figure 3. Diffuse-reflectance spectrum of **1**. Reference sample: barium sulfate.

Reflectance Spectrum. Because of the high insolubility of complex **1** in all common solvents, we studied its electronic spectroscopy in the solid state by measuring the spectrum in the diffuse-reflectance mode (Figure 3). The spectrum displays two broad intense bands in the visible region at 25.0×10^3 and 16.9×10^3 cm^{-1}, attributable to Cl → Fe^{III} ligand-to-metal charge transfer (LMCT) and Fe^{II} → bpym metal-to-ligand charge transfer (MLCT). In the related $Fe(bpym)_2(CN)_2$ compound, the Fe^{II} → bpym MLCT bands appear at 26.3 and 18.3 × 10^3 cm^{-1}, while the Cl → Fe^{III} LMCT bands have been

Table 3. Electronic Spectroscopic Data and TD-DFT Results

	exptl wavenumber/ 10^3 cm^{-1} (F(R))	calcd wavenumber/10^3 cm^{-1} (osc str)	main CI determinant contributions[a]	assignment
		17.1 (0.0105)	H(β) → L+2(β), H-1(β) → L(β), L+2(β)	LMCT, π Cl → dπ Fe^{III}
1	25.0 (0.25)	17.5 (0.0109)	H(β) → L+14(β), H-1(β) → L+13(β)	MLCT, dπ Fe^{II} → π bpym
		17.2 (0.0155)	H-6 (β) → L+1 (β), L (β), H-7 (β) → L (β)	LL′CT, π Cl → π bpym
		16.5 (0.0124)	H-5(β) → L+6(β), H-9(β) → L+7(β)	LMCT, π Cl → dπ Fe^{III}
		16.4 (0.0086)	H(β) → L+12(β)	MLCT, dπ Fe^{II} → π bpym
	not resolved	14.5 (0.0047)	H-1 (β) → L+3(β)	MMCT, dπ Fe^{II} → dπ Fe^{III}
		13.7 (0.0040)	H(β) → L+6(β), L+8(β), H-1(β) → L+7(β)	
		13.5 (0.0010)	H(β) → L+4(β), H-1(β) → L+5(β)	
		12.8 (0.0013)	H(β) → L+6(β), L+8(β), H-1(β) → L+3(β)	
	16.9 (0.15)	11.9 (0.0057)	H(β) → L+1(β), L(β), H-1(β) → L(β)	MLCT, dπ Fe^{II} → π bpym
		10.0 (0.0087)	H(β) → L+27(β), L+2(β), H-1(β) → L+28(β)	dπ Fe^{II} → dπ Fe^{II} MLCT, dπ Fe^{II} → π bpym
		9.1 (0.0189)	H(β) → L(β), L+1(β), H-1(β) → L(β)	MLCT, dπ Fe^{II} → π bpym
	8.3 (0.008)	1.6 (0.0027)	H(β) → L+19(β), L+22(β), L+2(β), H-1(β) → L+21(β), L+9 (β)	dπ Fe^{II} → dπ Fe^{II}
Fe(bpym)$_2$Cl$_2$		18.1 (0.0089)	H(β) → L+4(β), L+5(β)	MLCT, dπ Fe^{II} → π bpym
		11.0 (0.0138)	H(β) → L(β), L+6(β)	MLCT, dπ Fe^{II} → π bpym dπ Fe^{II} → dπ Fe^{II}
		1.4 (0.0007)	H(β) → L(β), L+3(β), L+4(β), L+6(β), L+7(β)	dπ Fe^{II} → dπ Fe^{II} MLCT, dπ Fe^{II} → π bpym
Fe(bpym)Cl$_3$(H$_2$O)		20.4 (0.0058)	H-2(β) → L+1(β), H-3(β) → L+1(β), H-4 → L+2(β), H-7(β) → L+2(β)	LMCT, π Cl → dπ Fe^{III}

[a] |CI| coefficients > 0.3.

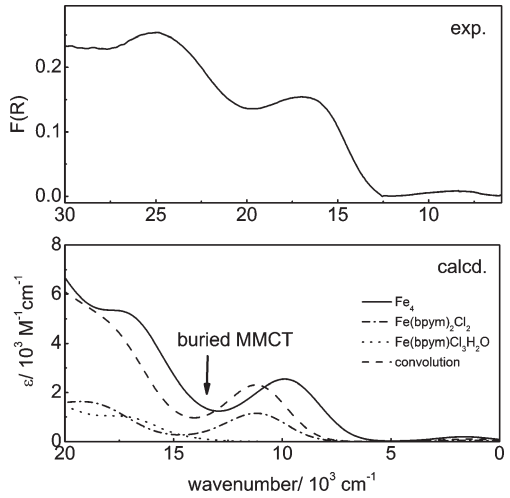

Figure 4. TD-DFT-calculated spectra, at the B3LYP level with a LanL2DZ basis set in vacuum, of complex **1** and its constituent fragments Fe(bpym)$_2$Cl$_2$ and Fe(bpym)Cl$_3$H$_2$O. The wavenumber range of calculated spectra is shown to shift with respect to the experimental one according to the linear correlation found (Figure S5 in the SI) between them.

observed in the range (40.0−25.0) × 10^3 cm^{-1} for several chloride ferric species.[10,11] An additional much less intense band can be observed in the near-IR (NIR) region at 8.3 × 10^3 cm^{-1} with a visible shoulder at the high energy side (ca. 10.0 × 10^3 cm^{-1}). The latter features are commonly observed in a high-spin d^6 Fe^{II} ion at this energy region and correspond to the low-symmetry split ^5E_g → $^5T_{2g}$ d−d unique spin-allowed transition.[11] For example, they are observed at 8.5 and 10.5 × 10^3 cm^{-1} in the related complex *cis*-Fe(phen)$_2$Cl$_2$.[11] Because of the impossibility to perform a spectroelectrochemistry experiment in solution, we decided to perform time-dependent DFT (TD-DFT) calculations to support the electronic spectral band assignments and explore the lack of an intervalence Fe^{II} → Fe^{III} metal-to-metal charge-transfer (MMCT) band expected in this type of mixed-valent compound.[12] The calculated electronic spectrum of **1** (Figure 3 and Table 3) is quite convincing and supports the presence of an intervalence charge-transfer (IVCT) active transition in the spectrum but buried under the LMCT and MLCT bands because of its low intensity.

All of the expected band assignments are supported by the calculations, with predominant LMCT, MLCT, and Fe^{II} d−d bands (Figure 4). The additional calculated electronic spectra of the isolated neutral moieties *cis*-Fe(bpym)$_2$Cl$_2$ and Fe(bpym)Cl$_3$(H$_2$O) show that the complex **1** spectral profile closely resembles the rough summation of the individual spectral contributions of both building fragments. The band profiles and relative intensities of the calculated spectrum nicely reproduce the experimental one, differing only in a fixed factor (ascribable to intrinsic DFT limitations), as demonstrated by the tight linear correlation (with a unitary slope) between the experimental and calculated transition energies (see the SI).

The apparent low intensity of the unobserved Fe^{II} → Fe^{III} MMCT seems to originate in the low overlap between the dπ donor and acceptor orbitals set as inferred from the molecular orbitals (MOs) involved in this transition calculated by TD-DFT (Figure 5). The cis arrangement of the Fe(bpym)$_2$Cl$_2$ moieties might be responsible for this symmetry mismatching.

Mössbauer Spectrosocopy. Zero-field Mössbauer spectra of complex **1** were measured at 80, 180, and 297 K (Figure 6). The spectral parameters obtained from a least-squares fit to the experimental points, assuming Lorentzian absorption lines, are summarized in Table 4.

(10) Ruminski, R. R.; Vantassel, K. D.; Petersen, J. D. *Inorg. Chem.* **1984**, *23*, 4380.
(11) Lever, A. B. P. *Inorganic Electronic Spectroscopy*, 2nd ed.; Elsevier Science Publishers BV: Amsterdam, The Netherlands, 1984.
(12) D'Alessandro, D. M.; Keene, F. R. *Chem. Rev.* **2006**, *106*, 2270.

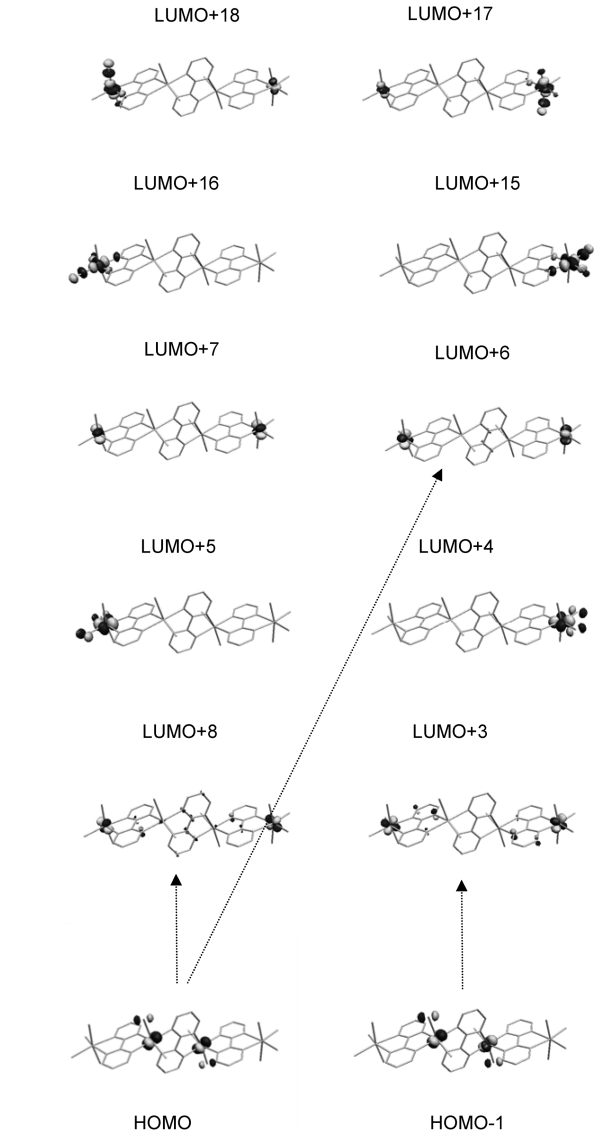

Figure 5. Main CI MOs contributing to the calculated MMCT transition. Arrows indicate the more intense contributions.

The spectrum of **1** at 80 K consists of two, 1:1 integrated area, nested quadrupole split doublets consistent with two different Fe sites and the centrosymmetric structure of **1** (also supported by the rather small line-width values). The isomer shifts of the two doublets are 0.49 and 1.14 mm s^{-1}, in the range expected for six-coordinated high-spin Fe^{III} and Fe^{II} ions, respectively,[13] and in agreement with a localized mixed-valence species description. The distinctly different quadrupole splittings, ΔE_Q, of 0.29 and 2.56 mm s^{-1} are in the range observed for high-spin d^5 Fe^{III} ions and high-spin d^6 Fe^{II} ions in comparable environments. For example, ΔE_Q values observed for $FeCl_3$, $FeCl_3 \cdot 6H_2O$, $FeCl_2 \cdot H_2O$, and $Fe(phen)_2Cl_2$ are 0, 0.97, 2.03, and 3.28 mm s^{-1}, respectively.[13]

With increasing temperature, the two-doublet feature is retained and the line widths almost keep the same small values. The smooth decrease observed for both Fe sites in the isomer shifts, with increasing temperature, is expected for a second-order Doppler shift.[14] Regarding the other key parameter ΔE_Q, Fe^{III} site quadrupole splitting is unchanged with increasing temperature, while the ΔE_Q value for the Fe^{II} doublet decreases from 2.56 to 1.92 mm s^{-1} upon heating to 297 K. This shifting is typical for high-spin ferrous systems because of changes in the Boltzmann populations of the low-lying electronic states that form as a consequence of spin−orbit and low-symmetry crystal-field perturbations.[15]

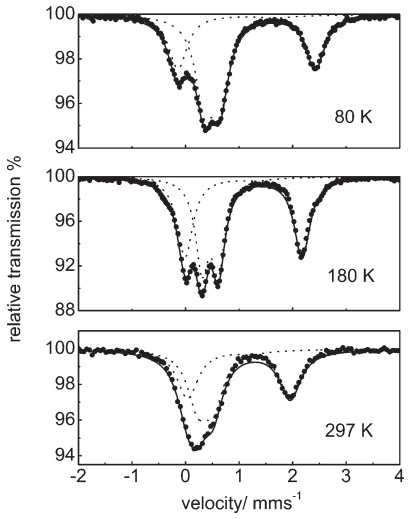

Figure 6. Mössbauer spectra at different temperatures of complex **1**. Full line: fitted convoluted spectra. Dashed lines: fitted Lorentzian doublets for each Fe site.

Table 4. Mössbauer Spectra Fitted Parameters

	site I			site II		
T/K	δ [mm s^{-1}]	ΔE_Q [mm s^{-1}]	$\Gamma/2$ [mm s^{-1}]	δ [mm s^{-1}]	ΔE_Q [mm s^{-1}]	$\Gamma/2$ [mm s^{-1}]
80	0.49	0.29	0.19	1.14	2.56	0.21
180	0.46	0.31	0.15	1.08	2.18	0.18
297	0.37	0.29	0.22	1.00	1.92	0.24

Overall, a mixed-valent localized picture for this Fe_4 compound is suggested from Mössbauer data up to room temperature.

Magnetic Properties. The direct-current (dc) magnetic susceptibility of complex **1** was measured in the temperature range 2−300 K (Figure 7) under an applied field of 1 T. At 300 K, a $\chi_m T$ (χ_m = molar susceptibility) value of 14.61 cm^3 K mol^{-1} is observed, quite close to the expected value for two isolated high-spin Fe^{III} ions ($S = {}^5/_2$) and two isolated high-spin Fe^{II} ions ($S = 2$), 14.76 cm^3 K mol^{-1} with $g = 2$. With decreasing temperature, the $\chi_m T$ product continuously decreases, approaching a zero value, and finally reaches a value of 0.89 cm^3 K mol^{-1} at 2 K. This behavior clearly indicates that antiferromagnetic interactions (weak ones as inferrd from the $\chi_m T$ value at 300 K) are operative between the Fe centers. This magnetic behavior has been previously observed in tightly related bipyrimidine-bridged Fe complexes, as in the

(13) Gutlich, P.; Ensling, J. In *Inorganic Electronic Structure and Spectroscopy*; Solomon, E. I., Lever, A. B. P., Eds.; Wiley-VCH: New York, 1999; Vol. *1*.

(14) Lynch, M. W.; Valentine, M.; Hendrickson, D. N. *J. Am. Chem. Soc.* **1982**, *104*, 6982.

(15) (a) Reiff, W. M.; Dockum, B.; Weber, M. A.; Frankel, R. B. *Inorg. Chem.* **1975**, *14*, 800. (b) Stassinopoulos, A.; Schulte, G.; Papaefthymiou, G. C.; Caradonna, J. P. *J. Am. Chem. Soc.* **1991**, *113*, 8686.

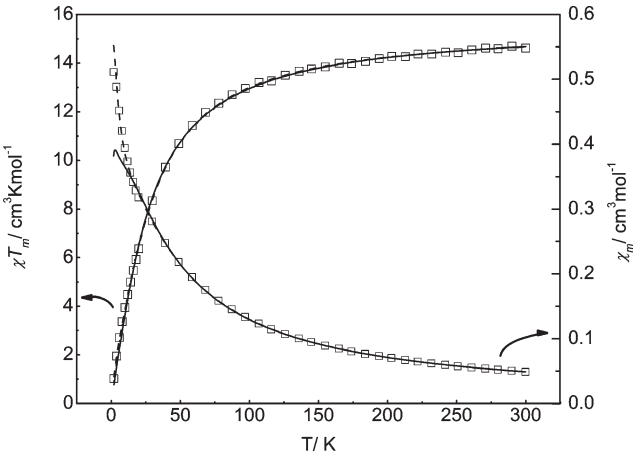

Figure 7. $\chi_m T$ and χ_m vs T plot at 1 T in the range 2−300 K of complex **1**. Full line: best fitting with the Hamiltonian of eq 1. Dashed line: best fitting with the Hamiltonian of eq 1 and zfs Hamiltonian of eq 2 (see the text).

Scheme 1. Exchange Coupling Pattern Describing Magnetic Interactions in Complex **1**

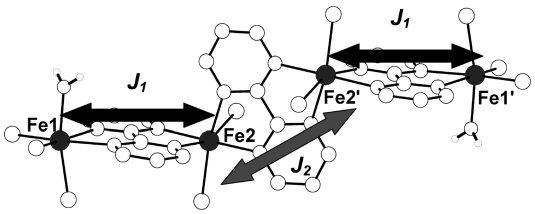

already mentioned dinuclear Fe^{II} complex **3**, [{Fe^{II}(bpym)Cl_2}$_2$-μ(bpym)], and the dinuclear Fe^{III} compound **4**, [{$FeCl_3$(H_2O)}$_2$-μ(bpym)].[2,3]

We attempted a full fitting of the data employing the *MAGPACK* package[16], where the energy of the different spin levels is obtained through diagonalization of the suitable Hamiltonian. In this case, the Heisenberg spin Hamiltonian (with the corresponding Zeeman terms) describing the isotropic exchange interactions within this Fe_4 complex (Scheme 1) is given by eq 2, where J_1 refers to the interactions between the Fe^{III}−Fe^{II} pairs and J_2 refers to the Fe^{II}−Fe^{II} interaction:

$$\hat{H} = -2J_1(\hat{S}_{Fe1}\cdot\hat{S}_{Fe2} + \hat{S}_{Fe1'}\cdot\hat{S}_{Fe2'}) - 2J_2(\hat{S}_{Fe2}\cdot\hat{S}_{Fe2'}) \quad (1)$$

Both Fe^{III}−Fe^{II} exchange interactions must be identical because of the crystallographically imposed inversion center. A satisfactory fitting of the $\chi_m T$ vs T experimental data in the whole temperature range was obtained (Figure 7) with the following parameters: $g_{av} = 2.06 \pm 0.01$, $J_1 = -2.0 \pm 0.6$ cm^{-1}, and $J_2 = -1.9 \pm 0.6$ cm^{-1} ($R = 3.32 \times 10^{-4}$). These values for the exchange coupling constants J_{Fe-Fe} are in agreement with the previously found values in complexes **3** ($J_{Fe^{II}-Fe^{II}} = -1.1$ cm^{-1}) and **4** ($J_{Fe^{III}-Fe^{III}} = -0.4$ cm^{-1}).[2,3] It must be noticed at this point that an indistinguishable fit of the data can be obtained by applying the restraint $J_1 = J_2$, with parameters $g_{av} = 2.06 \pm 0.01$ and $J_1 = -1.99 \pm 0.05$ cm^{-1}. This can be better understood as an equivalence of both J values rather than a sort of overparameterization, as can be seen in a J_1−J_2 correlation error surface (see the SI).

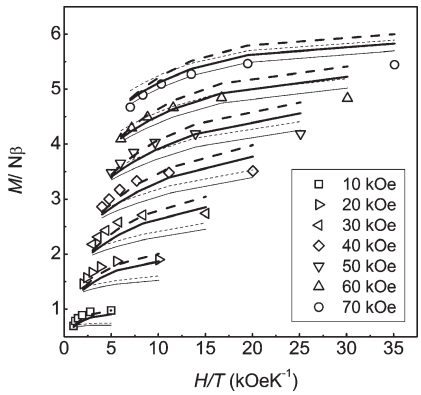

Figure 8. M vs H/T plot of complex **1** in the ranges 2−5 K and 10−70 kOe. The lines correspond to simulated and/or fitted plots (see the text): gray full line, Hamiltonian eq 1 with fixed $\chi_m T$ vs T best-fitting parameters; gray dashed line, Hamiltonian eq 1 with a fixed g_{av} value; black dashed line, Hamiltonian eq 1 and zfs eq 2 with fixed $\chi_m T$ vs T best-fitting parameters; black full line, Hamiltonian eq 1 and zfs eq 2 with fixed $\chi_m T$ vs T best-fitting J_1 and J_2 parameters.

However, below 15 K, the fit of the data is poor and the simulated data underestimate the experimental data. This discrepancy cannot be attributed to intermolecular antiferromagnetic exchange between adjacent Fe_4 clusters, mediated by hydrogen bonding (see the Structural Characterization section), as previously observed in the related dinuclear compound **4**[2] because this interaction should lower the χ_m data at low T. The most reasonable explanation must rely on the well-known single-ion zero-field-splitting (zfs) contribution of the high-spin d^6 Fe^{II} sites. In fact, this contribution is observed in the susceptibility data of the dinuclear complex **3**, [{Fe^{II}(bpym)Cl_2}$_2$-μ(bpym)], where a negative D value of about 17 cm^{-1} must be included to properly account for the experimentally observed data at low temperature.[3] When the proper zfs Hamiltonian term (eq 2) is added to eq 1, the best data-fitting parameters become $g_{av} = 2.05 \pm 0.01$, $J_1 = -2.2 \pm 0.2$ cm^{-1}, $J_2 = -0.6 \pm 0.2$ cm^{-1}, and $D = 17 \pm 1$ cm^{-1} ($R = 1.14 \times 10^{-4}$).

$$\hat{H}_{zfs} = D\{[\hat{S}^2_{Fe1} - S_{Fe1}(S_{Fe1}+1)/3] + [\hat{S}^2_{Fe1'} - S_{Fe1'}(S_{Fe1'}+1)/3]\} \quad (2)$$

The low-temperature χ_m data are now nicely reproduced (Figure 7), while only the Fe^{II}−Fe^{II} J_2 exchange coupling constant value is somewhat lower than the value obtained with complete neglect of the zfs term. In spite of certain overparameterization risks, no strong correlation is observed between J_1, J_2, and D parameters, as can be observed in the respective contour error plots (see the SI). From these same plots, it can also be noticed that the alternative set of parameters with a negative D value affords local minima with much poorer goodness of fit values.

From both negative exchange coupling constant values, a diamagnetic $S = 0$ ground state is established. However, low-energy-lying magnetic states are expected because of the weak magnitude of both J parameters. Precisely, when the zfs effects on the energy level diagrams are omitted (see

(16) Borras-Almenar, J. J.; Clemente-Juan, J. M.; Coronado, E.; Tsukerblat, B. S. *J. Comput. Chem.* **2001**, *22*, 985.

the SI), the first excited state is $S = 1$ at only 1.3 cm^{-1} from the ground state, followed by $S = 2$ at 5.7 cm^{-1}.

In order to obtain more information about the low-lying energy levels and of the single-ion zfs contribution of Fe^{II} sites, we performed magnetization measurements in the range 2−5 K under external magnetic fields up to 70 kOe (Figure 8). No superimposed isofield magnetization curves are observed. The maximum reduced magnetization value reached at 2 K and 70 kOe is 5.44 Nβ, close to the expected saturation value for a pure spin $S = 3$ with a g value of around 2.0. This M vs H/T profile is in agreement with a diamagnetic ground state with low-lying magnetic excited states, allowing energy level crossing. In fact, when the energy levels plot is inspected (see the SI), it is found that two crossings are probable around 15 kOe ($S = 1$) and 45 kOe ($S = 2$). At the maximum scanned field of 70 kOe, an additional excited state with $S = 3$ appears as the first low-lying excited state very close in energy to that of the ground state. This ground-state progression from $S = 0$ to almost $S = 3$ is in agreement with the observed progression of the saturation values of the increasing field individual isofield lines. Of course, at this point, we completely neglect further energy level splittings due to zfs contribution, which could certainly modify this description, but the present model allows a qualitative understanding of the reduced magnetization plot profiles.

Modeling of the magnetization curves employing *MAGPACK*, with eq 2 Hamiltonian, and no zfs contribution is poor (Figure 8), even when independent J_1 and J_2 values are fitted. Fixing $g_{av} = 2.06$ best values of $J_1 = -1.9 \pm 0.8$ cm^{-1} and $J_2 = -1.6 \pm 0.9$ cm^{-1} affords an agreement factor $R = 1.5 \times 10^{-3}$ but a poor low-field description. A clear improvement is achieved if the zfs contribution is included (eq 2), employing best-fitting parameters obtained from $\chi_m T$ vs T data ($R = 1.2 \times 10^{-3}$) or fixing just J_1 and J_2 and fitting the g_{av} and D parameters. In the latter case, optimized parameters found are $g_{av} = 2.08 \pm 0.02$ and $D = 12 \pm 1$ cm^{-1} ($R = 1.2 \times 10^{-3}$).

Magnetization data support again a positive D value for the local zfs Fe^{II} contribution. It seems at least striking that just the opposite sign for the D value has been determined for the structurally related complex **3**, [{Fe^{II}(bpym)Cl_2}$_2$-μ(bpym)].[3] Only a few examples of unequivocal determinations of the D sign in high-spin Fe^{II} systems are reported, and both possible alternatives have been found.[17,18] A similar positive D value was found for a related *cis*-bis(thiazoline)iron(II) complex.[18] In the case of complex **1**, the local pseudosymmetry of the Fe^{II} sites is roughly C_2, and the splitting of ground state $^5T_{2g}$ results in three orbital nondegenerate new quintuplets: ^{5}B, ^{5}B, and ^{5}A. A further spin−orbit coupling interaction determined these quintuplets as zfs. The relative ligand-field strengths of the Fe^{II} coordination sphere (angle- and distance-dependent) conclude the final D sign as a first approximation. More experimental data (high-field electron paramagnetic resonance) or an elaborated theoretical approach must be performed to get a final definitive assessment regarding the sign and magnitude of the Fe^{II} zfs contribution.[9,19]

Table 5. DFT-Calculated Exchange Coupling Constants J for Complex **1**

	Ruiz formalism (Ising formalism)		experimental	
	LanL2DZ	TZVP	$\chi_m T$ data	M vs H/T data
J_1/cm^{-1}	−1.56 (−1.87)	−1.62 (−1.94)	−2.0 ± 0.6 −2.2 ± 0.2 (zfs)	−1.9 ± 0.8
J_2/cm^{-1}	−1.59 (−1.98)	−1.83 (−2.30)	−1.9 ± 0.6 −0.6 ± 0.2 (zfs)	−1.6 ± 0.9

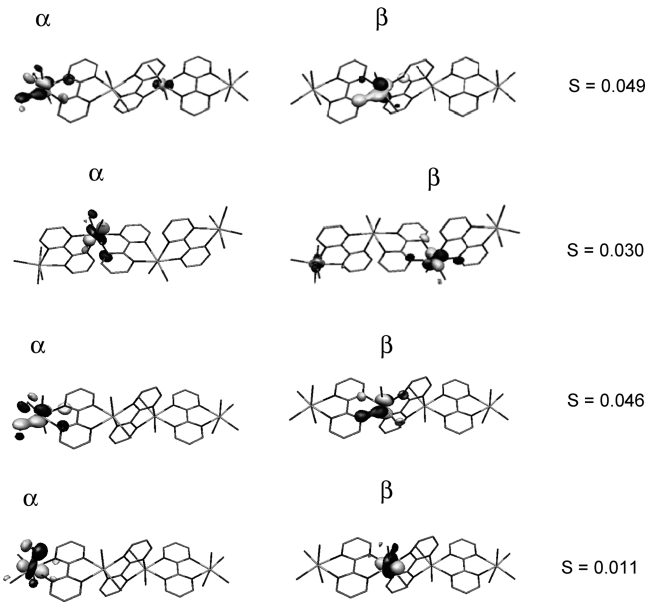

Figure 9. Magnetic orbitals after a COT describing the J_1 and J_2 exchange interactions.

Complementary DFT broken-symmetry calculations were performed to obtain theoretical exchange coupling constant values and to inspect the nature of the exchange pathways in terms of magnetic orbital descriptions. The J_1 and J_2 calculated values with two different basis sets and the two different spin formalism approaches employed are listed in Table 5.

It can be noticed that very close values are obtained for J_1 and J_2, both in good agreement with the experimental findings, independent of the method or basis set used. Simulated $\chi_m T$ vs T plots employing these theoretical values show excellent results (see the SI). These theoretical calculations support the weak antiferromagnetic interactions between Fe centers, as was expected for the bpym ligand. The nonzero overlapping magnetic orbitals for the Fe^{II} and Fe^{III} sites are shown in Figure 9, represented through the corresponding orbital transformation. Both broken-symmetry topology contributions have been merged into a unique set of α−β pairs.

As was also verified in some previous bpym-bridged examples, the main operative exchange pathways rely on pure σ-type orbital overlaps between the metal centers

(17) (a) Knapp, M. J.; Krzystek, J.; Brunel, L. C.; Hendrickson, D. N. *Inorg. Chem.* **2000**, *39*, 281. (b) Carver, G.; Tregenna-Piggott, P. L. W.; Barra, A. L.; Neels, A.; Stride, J. A. *Inorg. Chem.* **2003**, *42*, 5771. (c) Telser, J.; van Slageren, J.; Vongtragool, S.; Dressel, M.; Reiff, W. M.; Zvyagin, S. A.; Ozarowski, A.; Krzystek, J. *Magn. Reson. Chem.* **2005**, *43*, S130.

(18) Ozarowski, A.; Zvyagin, S. A.; Reiff, W. M.; Telser, J.; Brunel, L. C.; Krzystek, J. *J. Am. Chem. Soc.* **2004**, *126*, 6574.

(19) Krzystek, J.; Ozarowski, A.; Telser, J. *Coord. Chem. Rev.* **2006**, *250*, 2308.

and the bpym ligand.[8,20] Because of the local low symmetry, the d orbitals involved are not the expected d_σ and d_π sets but just combinations of them. The similar overlap integrals describing $Fe^{III}-Fe^{II}$ and $Fe^{II}-Fe^{II}$ exchange interactions justified the close values obtained for J_1 and J_2 isotropic constants.

Conclusion

We have successfully prepared the first example of a polynuclear discrete coordination compound exhibiting only bpym bridges and containing a first-row d transition metal. All spectroscopic data show that this is a valence-localized mixed-valent $Fe^{II}-Fe^{III}$ cluster with typical Mössbauer lines for both sites and not an experimental observed but a theoretically predicted weak high-energy IVCT transition. Regarding the magnetic properties, the high-spin Fe^{II} and Fe^{III} ions interact in a weakly antiferromagnetic way with isotropic J constants of a few wavenumbers.

To our knowledge, this is just the second example of a structurally characterized discrete polynuclear complex with all bpym bridges and the first mixed-valent one. In this sense, the complex **1** structure becomes a remarkable breakthrough in the field of polynuclear transition-metal cluster compounds, and it may become a milestone for these types of systems. The smooth self-assembly one-pot synthetic route leaves the door open for further exploration of these types of complexes, which occupy the vacant place between dinuclear and coordination polymer bpym-bridged systems.

Experimental Section

Material and Physical Measurements. The ligand 2,2′-bipyrimidine (bpym) was prepared following a previously reported procedure.[21] All other chemicals were reagent grade and were used as received without further purification. Elemental analysis for C, H, and N was performed on a Foss Heraeus Vario EL elemental analyzer. UV−vis−NIR spectra were recorded with a Cary 5E spectrophotometer using the diffuse-reflectance technique with barium sulfate as a reference. Magnetic measurements were performed with a Quantum Design MPMS XL SQUID magnetometer. dc measurements were conducted from 2 to 300 K at 1 T and from 2 to 5 K under an applied field up to 7 T. All measurements were performed on restrained polycrystalline samples in order to avoid field-induced reorientation of the microcrystals. Experimental magnetic data were corrected for diamagnetism of the sample holders and of the constituent atoms (Pascal's tables). Mössbauer data were recorded on an alternating-current constant-acceleration spectrometer. The minimum experimental line width was 0.3 mm s^{-1} (full width at half-height). The sample temperature was maintained constant in an Oxford Instrument. Isomer shifts are quoted relative to iron metal at 300 K.

Synthesis of the Complex *cis*-$[Cl_3(H_2O)Fe^{III}(bpym)]_2$-$\mu$(bpym)$Fe^{II}Cl_2(bpym)]_2\cdot H_2O$ (1). A total of 0.35 g (1.3 mmol) of $FeCl_3\cdot 6H_2O$ and 0.26 g (1.3 mmol) of $FeCl_2\cdot 4H_2O$ were dissolved jointly in 30 mL of methanol to afford a clear orange solution. Separately, 0.31 g (2.0 mmol) of bpym was dissolved in 20 mL of acetonitrile. Both solutions were mixed, and a new dark-red solution was obtained. After 30 min, it was filtered to remove a dark insoluble (not further characterized) solid, and the resulting clear solution was left undisturbed to slowly evaporate at room temperature. After a few days, dark-red block crystals of **1**, suitable for X-ray measurement, were obtained. One specimen was collected for diffraction experiments, and the remaining material was collected by filtration and air-dried. The dried solid had only one solvation water molecule, in contrast with crystals, which have two crystallization water molecules. Yield: 0.138 g (20%). Anal. Calcd for $C_{24}H_{24}Cl_{10}Fe_4N_{12}O_3$: C, 26.05; H, 2.19; N, 15.19. Found: C, 26.05; H, 2.66; N, 15.32.

X-ray Structure Determination. Crystals suitable for X-ray diffraction were obtained directly from the synthetic procedure and mounted in a glass fiber. The crystal structure was determined with a Bruker Smart APEX II CCD area detector diffractometer using graphite-monochromated Mo Kα radiation ($\lambda = 0.710\,73$ Å) at 173 K. Data were corrected for absorption with *SADABS*.[22] The structures were solved by direct methods with *SHELXS-97*[23] and refined by full-matrix least squares on F^2 with anisotropic displacement parameters for non-hydrogen atoms with *SHELXL-97*.[23] Hydrogen atoms were added geometrically and refined as riding atoms with a uniform value of U_{iso}, with the exception of hydrogen atoms of coordinated and free water molecules that were located in the difference map. Crystallographic and refinement data are shown in Table 1.

CCDC 776615 contains the supplementary crystallographic data for this paper. These data can be obtained free of charge from the Cambridge Crystallographic Data Centre via www.ccdc.cam.ac.uk/data_request/cif.

DFT Quantum Computations. DFT spin-unrestricted calculations were performed at the X-ray geometry using the *Gaussian03* package (revision D.01)[24] at the B3LYP level employing the medium-size LanL2DZ basis set and the more complete TZVP one. Tightly converged (10^{-8} Eh in energy) single-point calculations were performed in order to analyze the exchange coupling between the metallic ion centers. The methodology applied here relies on the broken-symmetry formalism, originally developed by Noodleman for self-consistent-field methods,[25] which involves a variational treatment within the restrictions of a single spin-unrestricted Slater determinant built upon using different orbitals for different spins. This approach has been later applied within the framework of DFT.[26] The high-spin (HS) and broken-symmetry (BS) energies were then combined to estimate the exchange coupling parameter J involved in the widely used Heisenberg−Dirac−van Vleck (HDvV) Hamiltonian.[27] We have calculated the different spin topologies of broken-symmetry nature (see the SI) by alternately flipping the spin on the different metal sites (two different BS topologies in this case). The exchange coupling constants J_i can be obtained after the individual pairlike component spin interactions involved in the description of the different broken-symmetry states are considered. We used the two main methodologies reported: the Ising approach,[28] in which the broken-symmetry states were directly considered as eigenstates of the HDvV Hamiltonian with the corresponding equation

$$E_{BS} - E_{HS} = 2J_{12}(2S_1S_2)$$

and the method proposed by Ruiz and co-workers,[29] in which the following equation was applied:

$$E_{BS} - E_{HS} = 2J_{12}(2S_1S_2 + S_2), \text{ with } S_2 < S_1$$

(20) (a) Julve, M.; Demunno, G.; Bruno, G.; Verdaguer, M. *Inorg. Chem.* **1988**, *27*, 3160. (b) Albores, P.; Rentschler, E. *Dalton. Trans.* **2010**, *39*, 5005.
(21) Vlad, G.; Horvath, I. T. *J. Org. Chem.* **2002**, *67*, 6550.
(22) Sheldrick, G. M. *SADABS, Multiscan Absorption Correction Program*; University of Göttingen: Göttingen, Germany, 1996.
(23) Sheldrick, G. M. *SHELXS-97 and SHELXL-97, Programs for Crystal Structure Resolution*; University of Göttingen: Göttingen, Germany, 1997.
(24) Frisch, M. J.; et al. *Gaussian03*, revision D.01; Gaussian Inc.: Pittsburgh, PA, 2003.
(25) Noodleman, L. *J. Chem. Phys.* **1981**, *74*, 5737.
(26) Noodleman, L.; Baerends, E. J. *J. Am. Chem. Soc.* **1984**, *106*, 2316.
(27) Kahn, O. *Molecular Magnetism*; VCH: New York, 1993.
(28) Dai, D. D.; Whangbo, M. H. *J. Chem. Phys.* **2003**, *118*, 29.
(29) Ruiz, E.; Rodriguez-Fortea, A.; Cano, J.; Alvarez, S.; Alemany, P. *J. Comput. Chem.* **2003**, *24*, 982.

In both cases, a set of linear equations must be solved to obtain the *J* parameters.

Additionally, we have also employed the BS-type spin-unrestricted solutions after a corresponding orbital transformation (COT)[30] as a means to visualize the interacting nonorthogonal magnetic orbitals and, hence, the spin-coupling exchange pathways. These orbitals do not have a well-defined orbital energy; for this reason, orbital energies are not given explicitly but only their overlapping magnitudes. The TD-DFT computation at the X-ray geometry only with the medium-size LanL2DZ basis set was calculated for the HS state to assist in the interpretation and assignment of the electronic spectrum. The output contained information for the excited-state energies, oscillator strengths (*f*), and a list of transitions that give rise to each excited state. The orbitals involved as well as the orbital contribution coefficients of the transitions were obtained. The molar absorptivity was calculated with a full width at half-maximum of 3000 cm^{-1}. As an additional tool, we performed identical TD-DFT calculations for the complex **1** constituents, neutral isolated fragments $Fe^{III}(H_2O)Cl_3bpym$ and *cis*-$Fe^{II}(bpym)_2Cl_2$, with their geometries arising from the X-ray structure of the Fe_4 complex.

(30) Neese, F. *J. Phys. Chem. Solids* **2004**, *65*, 781.

Acknowledgment. We gratefully acknowledge the Alexander von Humboldt Foundation for granting a postdoctoral fellowship and Bernd Mienert for Mössbauer measurements. This work was partially supported by the National Center for Supercomputing Applications under Grant TG-MCA05S010. P.A. is a member staff of CONICET.

Supporting Information Available: ORTEP plot (50% probability) of molecular structure of complex **1**, showing an alternative staircase topology (Figure S1), ball-and-stick representation of the complex **1** crystal structure unit cell (Figure S2), ball-and-stick representation of intermolecular interactions in the complex **1** crystal structure (Figures S3 and S4), TD-DFT-calculated energy vs experimental transition correlation plot (Figure S5), J_1-J_2 error contour plots corresponding to the $\chi_m T$ vs T simulation (Figures S6 and S7), J_1-D error contour plot corresponding to the $\chi_m T$ vs T simulation (Figures S8 and S9), low-lying energy level plot (Figure S10), $\chi_m T$ vs T simulation with DFT-calculated J values (Figure S11), spin-density contours of the nonequivalent broken-symmetry spin states (Figure S12), and X-ray crystallographic file of complex **1** in CIF format. This material is available free of charge via the Internet at http://pubs.acs.org.